Supporting Information

Hydrogen-bonded CdSe/PDI with double electric field synergism for enhanced overall water splitting performance

Jinbo Xue,[*ab] Chengkun Lei,[ab] Qiurong Li,[ab] Zhe Sun,[ab] Huimin Li,[ab] Shihao Ding,[ab] Husheng Jia,[ab] Qianqian Shen,[*ab] Xuguang Liu[ab] and Yongfa Zhu[*c]

[a]*Key Laboratory of Interface Science and Engineering in Advanced Materials (Taiyuan University of Technology), Ministry of Education, Taiyuan 030024, China. E-mail address: xuejinbo@tyut.edu.cn, shenqianqian@tyut.edu.cn*

[b]*College of Materials Science and Engineering, Taiyuan University of Technology, Taiyuan 030024, P. R. China*

[c]*Department of Chemistry, Tsinghua University, Beijing 100084, China. E-mail address: zhuyf@tsinghua.edu.cn*

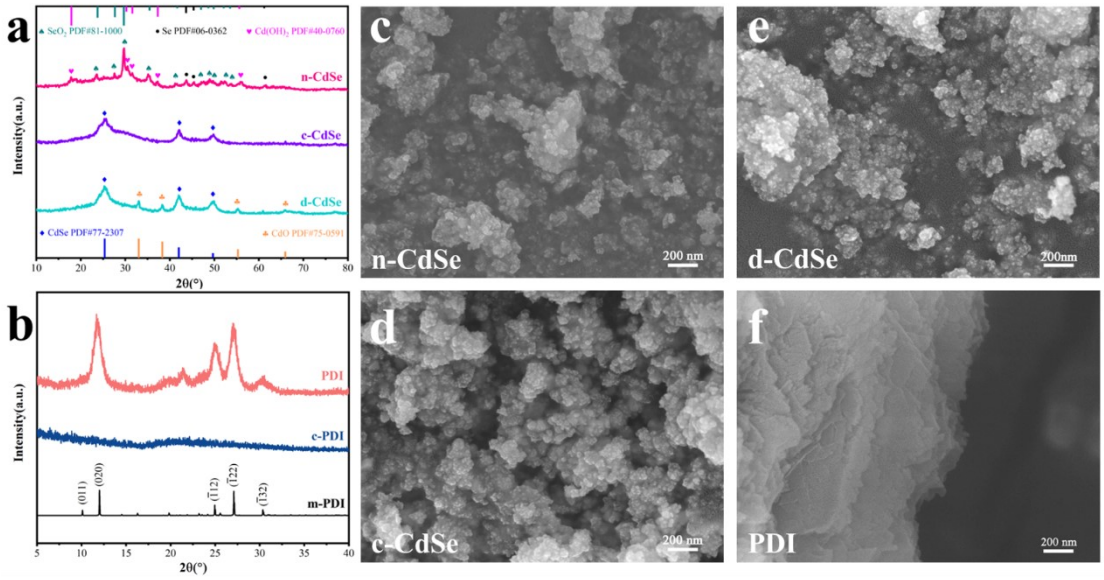

Fig. S1 XRD patterns of various CdSe (a) and PDI (b), SEM images of various CdSe (c–e) and PDI (f)

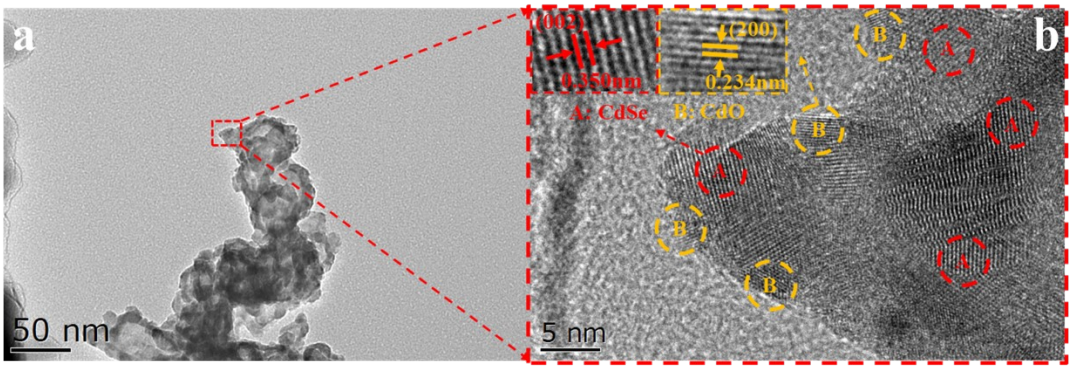

Fig. S2 TEM images (a) of d-CdSe and lattice fringes of d-CdSe (b)

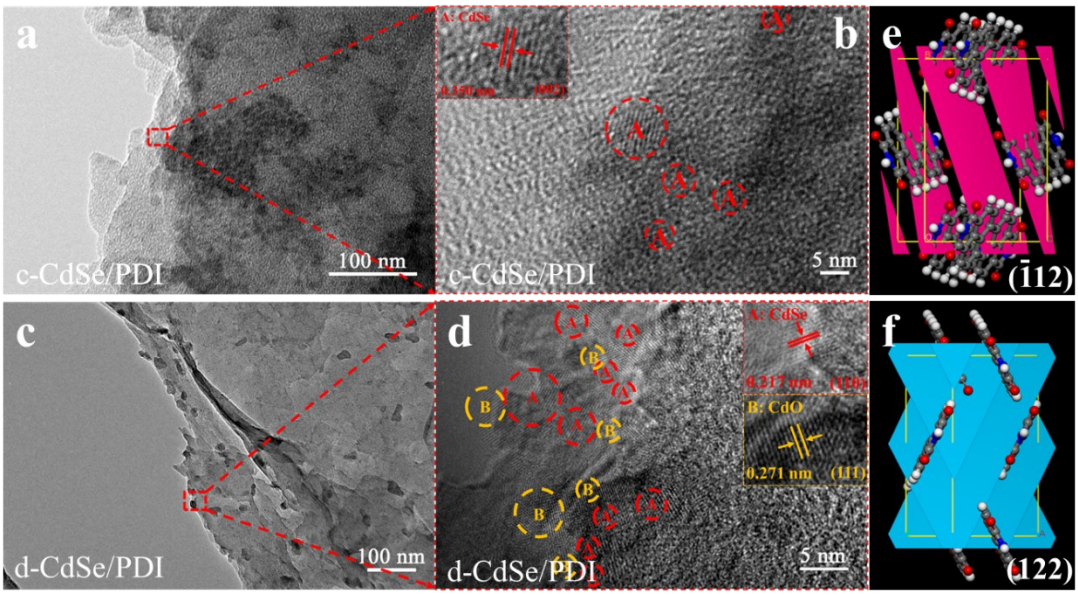

Fig. S3 TEM images of c-CdSe/PDI (a) and (b); TEM images of d-CdSe/PDI (c) and (d); and (−112) (e) and (122) (f) crystal faces of PDI

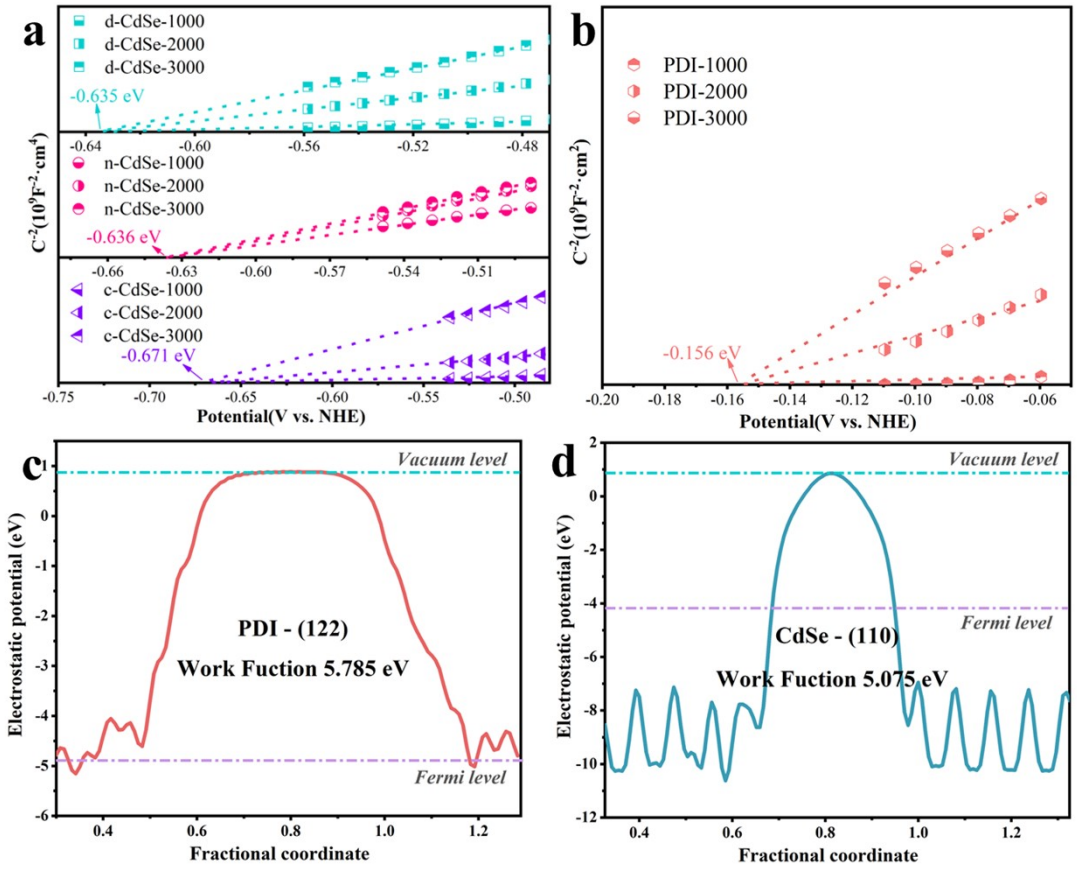

Fig. S4 Mott–Schottky curves of various CdSe (a) and PDI (b); DFT-calculated work function of PDI (122) (c) and CdSe (110) (d)

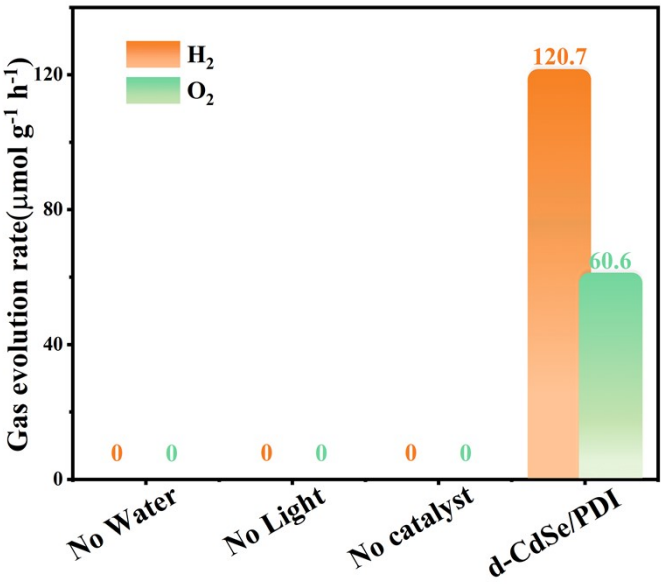

Fig. S5 Gas yield of control experiment

Table S1. Comparison of the photocatalytic water splitting activity for some representative photocatalysts

material	band gap	co-catalyst	light source	solution	gas generation rate(μmol g^{-1} h^{-1})	ref.
d-CdSe/PDI	1.6/2.8	--	300 W-Xe (> 380 nm)	10 mL H_2O	H_2:120.7 O_2:60.6	This work
Cu_7S_4/*r*-MnS	0.77/2.12	MnO_x	300 W-Xe (>420 nm)	6 mL H_2O	H_2:309 O_2:36	[S1]
Cu_2P/Bi_2WO_3	1.6/2.8	--	150 W-Xe	Na_2HPO_4/ NaH_2PO_4, 80 mL	H_2:4.7 O_2:2.3	[S2]
P/Bi_2VO_3	0.7/2.39	--	320 W-Xe (> 420 nm)	8 mL H_2O	H_2:16 O_2:102	[S3]
BP/RP	1.27/1.96	Co,Fe, Ni,Cu	200 W-LED (> 420 nm)	6 mL H_2O	H_2:300	[S4]
$ZnTe/TiO_2$	2.14/3.05	Au	320 W-Xe (> 350 nm)	50 mL H_2O	H_2:3340 O_2:1670	[S5]
C_{ring}/C_3N_4	0/2.74	3 wt%Pt	300 W-Xe (>420 nm)	Pure H_2O	H_2:150 O_2:75	[S6]
$g\text{-}C_3N_4/TiO_2$	2.7/3.2	--	300 W-Xe (> 400 nm)	100 mL H_2O	H_2:65	[S7]

The red part is this work, the blue part is the heterojunction composed of inorganic and inorganic materials, and the yellow part is the heterojunction formed by hybridization of organic and inorganic materials.

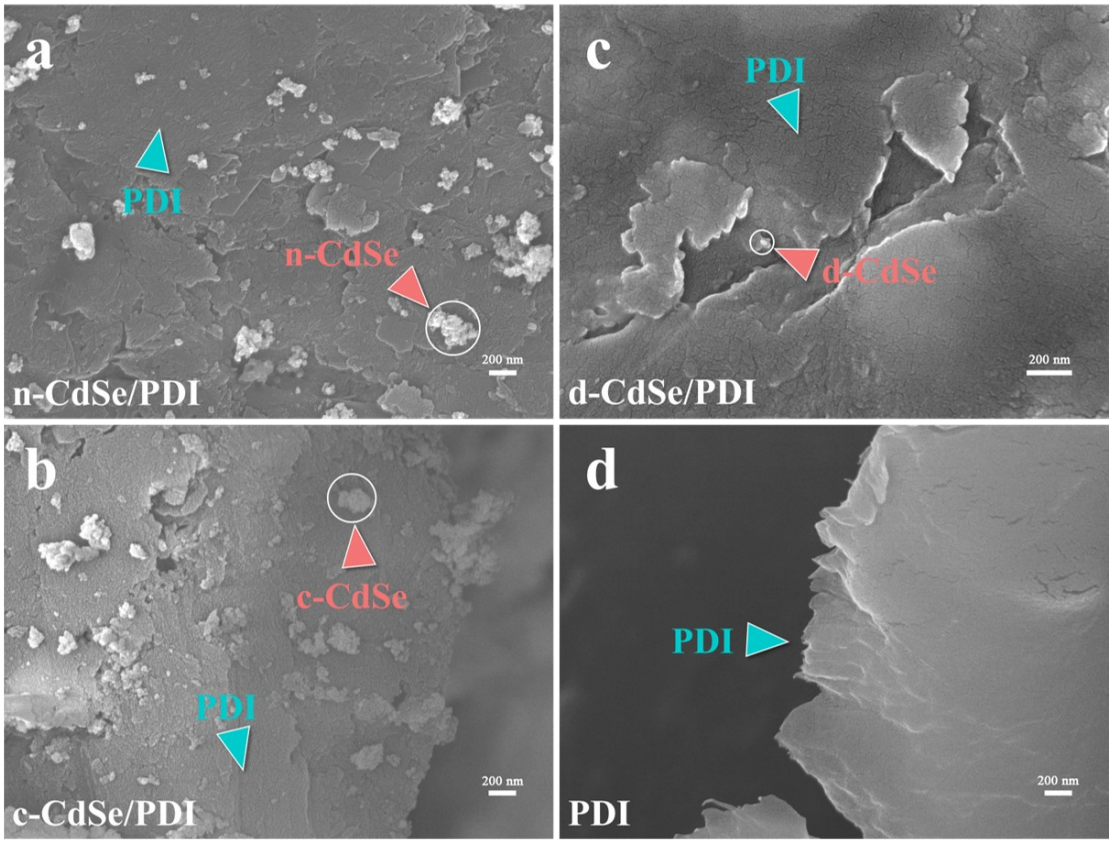

Fig. S6 SEM images of samples after reaction

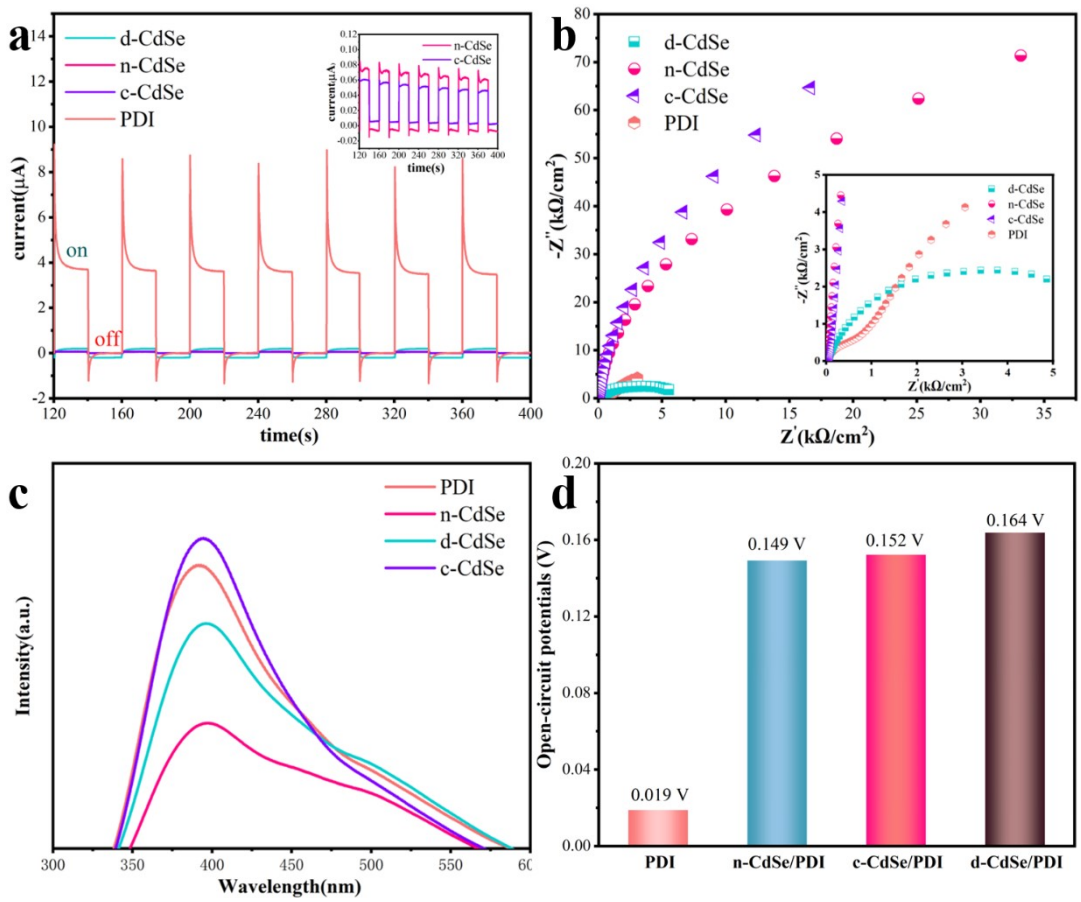

Fig. S7 *I-t* curves (a), EIS (b), and PL of single-compoment samples (c); open-circuit potential of PDI and composite samples (d)

The built-in electric field strength of the overall catalyst can be obtained from Eq. S1:[S8]

$$E = \left(\frac{-2V_s\rho}{\varepsilon\varepsilon_0}\right)^{1/2} \quad \text{..... Eq. S1}$$

where E is the internal electric field magnitude, V_s the surface voltage, ρ the surface charge density, $\mathcal{E}$ the low-frequency dielectric constant, and $\mathcal{E}_0$ the permittivity of free space. The above equation reveals that the internal electric field magnitude is mainly determined by the surface voltage and charge density because $\mathcal{E}$ and $\mathcal{E}_0$ are two constants.

The carrier lifetime in the TRPL can be calculated from Eq. S2:

$$\tau_{ave} = \frac{A_1\tau_1^2 + A_2\tau_2^2}{A_1\tau_1 + A_2\tau_2} \quad \text{..... Eq. S2}$$

where A_1 and A_2 represent the amplitudes of the fast and slow components, τ_1 and τ_2 the time constants. The fitting parameters used for our curves are listed in Table S2.

Sample	τ_1/ns	τ_2/ns	A_1/%	A_2/%	τ_{ave}/ns
d-CdSe	0.29	4.32	88.85	11.15	2.92
PDI	0.28	3.21	90.93	9.07	1.84
d-CdSe/PDI	0.29	4.72	87.74	12.26	3.37

Table S2. Fitting parameters for transient PL spectra

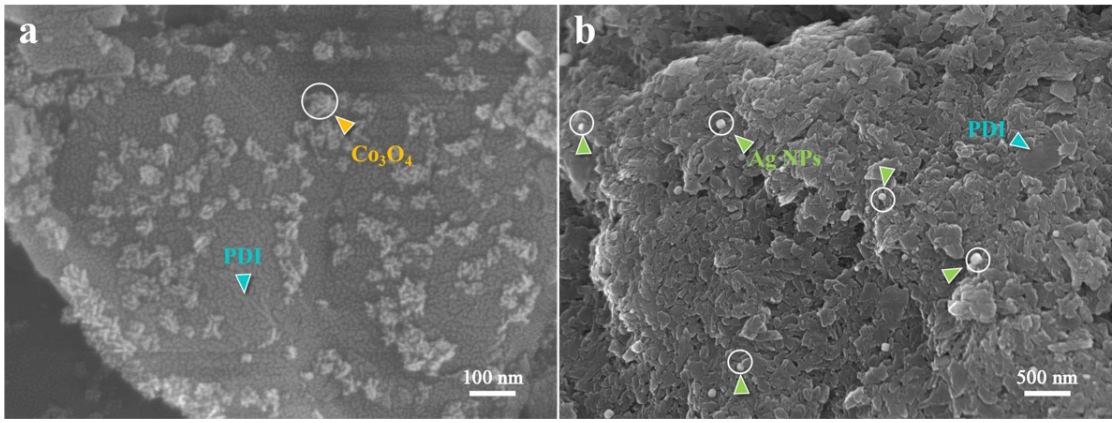

Fig. S8 Morphology of Co_3O_4 and Ag nanoparticles loaded on PDI, respectively

We determined the hole accumulation and electron accumulation surfaces of PDI by the position of photodeposited Co_3O_4 and Ag nanoparticles loaded on PDI nanosheets. The surface where Co_3O_4 is located is the hole accumulation surface, and the surface where Ag nanoparticles are located is the electron accumulation surface. It can be observed from Fig. S8 that Co_3O_4 is loaded on the front side of PDI nanosheets and Ag nanoparticles are loaded on the side of PDI nanosheets. Therefore, the side of PDI nanosheet (122) is the electron accumulation surface and the front side (−112) is the hole accumulation surface.

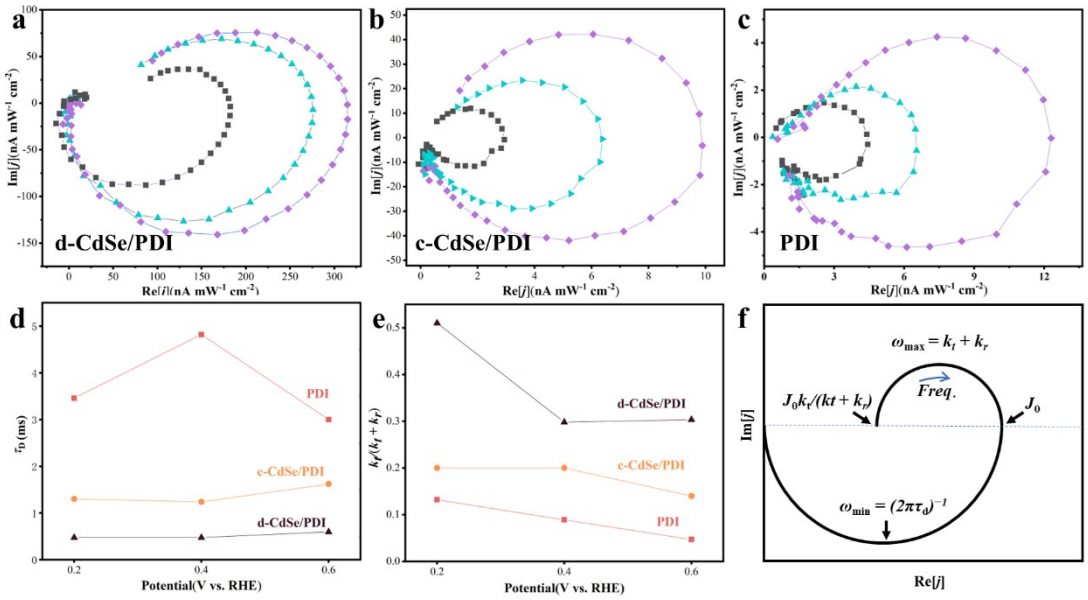

Fig. S9 IMPS of d-CdSe/PDI (a), c-CdSe/PDI (b), and PDI (c) measured at 0.2, 0.4 and 0.6 V vs. NHE; τ_D (d) and $k_t/(k_t + k_r)$ (e) values extracted from the IMPS fitting data at different potentials; and schematic diagram of the IMPS mathematical model (f)

Intensity-modulated photocurrent spectra (IMPS) allows further quantitative analysis of the carrier dynamics in the sample. The intensity-modulated photocurrent response $j(\omega)$ is shown in Eq. S3: [S9]

$$j(\omega) = j_0 \times \frac{k_t + i\omega(\frac{C_H}{1 + C_H/C_{SC}})}{k_t + k_r + i\omega} \times \frac{1}{1 + i\omega\tau_D} \quad \text{..... Eq. S3}$$

Where j_0 is the hole amplitude of the hole flow to the surface, C_{SC} and C_H are the point capacitances of the space charge layer and the Helmholtz layer, k_t and k_r are the pseudo-first-order rate constants for charge transfer and complexation, τ_D is the average transport time of the photogenerated electrons, ω is the frequency of the modulated light and i is the current. It can be seen from Fig. S9f that in the low-frequency semicircle, the real part at $\omega = 0$ is close to $j_0k_t/(k_t + k_r)$, and $\omega_{max} = k_t + k_r$ can satisfy its maximum value. The high-frequency intercept of the composite semicircle corresponds to the instantaneous photocurrent, and the value of the real part tends to j_0. The value of td is related to the frequency of the lowest point of the imaginary part. Therefore, the values of j_0, τ_D, k_t and k_r can be calculated from the high frequency intercept, the low frequency intercept, ω_{max} and ω_{min}. Typically, τ_D is considered to be a metric of charge bulk phase transport, and the larger its value, the higher the bulk phase complex.[S10] The degree of bulk-phase complexation can be derived from Fig. S9d: d-CdSe/PDI < c-CdSe/PDI < PDI. d-CdeSe/PDI has the strongest charge-transfer capability, as can be seen from the relative magnitude of the electron-transfer efficiency, $k_t/(k_t + k_r)$, in Fig. S9e. It further indicates that an isotropic double electric field can synergistically promote charge transfer and transport.

Reference

1 Y. Zhang, D. Wang, W. Liu, Y. Lou, Y. Zhang, Y. Dong, J. Xu, C. Pan and Y. Zhu, *Appl. Catal. B*, **2022**, 300, 120762.

2 A. Rauf, M. Ma, S. Kim, M.S.A.S. Shah, C.H. Chung, J. H. Park and P. J. Yoo, *Nanoscale*, **2018**, 10, 3026–3036.

3 M. Zhu, Z. Sun, M. Fujitsuka and T. Majima, *Angew. Chem. Int. Ed.*, **2017**, 130, 2182–2186.

4 F. Liu, R. Shi, Z. Wang, Y. Weng, C. Che and Y. Chen, *Angew Chem Int Ed.*, **2019**, 58, 11791–11795.

5 W. Zhang, Y. Hu, C. Yan, D. Hong, R. Chen, X. Xue, S. Yang, Y. Tian, Z. Tie and Z. Jin, *Nanoscale*, **2019**, 11, 9053–9060.

6 W. Che, W. Cheng, T. Yao, F. Tang, W. Liu, H. Su, Y. Huang, Q. Liu, J. Liu, F. Hu, Z. Pan, Z. Sun and S. Wei, *J. Am. Chem. Soc.*, **2017**, 139, 8, 3021–3026.

7 J. Pan, M. You, C. Chi, Z. Dong, B. Wang, M. Zhu, W. Zhao, C. Song, Y. Zheng and C. Li, *Int. J. Hydrog. Energy*, **2018**, 43, 6586–6593.

8 Y. Zhang, D. Wang, W. Liu, Y. Lou, Y. Zhang, Y. Dong and J. Xu, *Appl. Catal. B*, **2022**, 300, 120762.

9 E. A. Ponomarev and L. M. Peter, *J. Electroanal. Chem.*, **1995**, 396, 219–226.

10 P. Liu, L. F. Florian and B. Florent, *J. Mater. Chem. A*, **2019**, 7, 1669–1677.